



Detection of iron-bearing mineral assemblages in Nainarmalai granulite region, south India, based on satellite image processing and geochemical anomalies

Gopinathan P · Priyadarsi Roy · Subramani T · Karunanidhi D

Received: 7 December 2021 / Accepted: 12 March 2022 / Published online: 12 October 2022
© The Author(s), under exclusive licence to Springer Nature Switzerland AG 2022

Abstract Although India's large iron ore reserves are well known, there are still few studies and research on iron ore prospecting in smaller deposits or the deposits with lower grade. Remote sensing concepts are useful to target for mineral exploration, since it covers a large area at low cost. In this research spectral remote sensing and digital image processing of ASTER data to locate and delineate the regions with iron oxide-bearing soils in granulite terrain at Nainarmalai (southern India) that has hypothetical reserve 8.2 million tons of iron in sub-surface banded magnetite quartzites. The image-based study component involved pre-processing atmospheric correction and processing of the image data reminiscent of band

ratio and band mixture to locate iron-bearing soils. We used blending of bands 5/3 + 1/2 to delineate ferrous iron oxide, band combination of 2/1 to delineate ferric iron oxide, and band ratio of 5/4 to delineate the lateritic soil. Further, the linear spectral unmixing outcome of ASRER data was evaluated concerning the ground truth of geochemical compositions of samples from the study area. Our results showed that image processing of the ASTER satellite data has the potential to delineate ferric, ferrous, and lateritic mineral assemblages in the iron-bearing soils with minimal requirement of ground truth verification. This research work aided in increasing trust in the use of space-based data for mineral prospecting. Image processing has demonstrated that ASTER data can be used to enhance iron ore exploration and the discovery of new mineralized areas.

G. P (✉)
CSIR-Central Institute of Mining and Fuel Research,
(Ministry of Science & Technology, Govt. of India),
Dhanbad, Jharkhand 826015, India
e-mail: srigopi555@gmail.com

P. Roy
Instituto de Geología, Universidad Nacional Autónoma de
México, Ciudad Universitaria, 04510 Ciudad de Mexico,
CP, Mexico

S. T
Department of Geology, College of Engineering, Anna
University, Chennai 600025, India

K. D
Department of Civil Engineering, Sri Shakthi Institute
of Engineering and Technology (Autonomous),
Coimbatore 641062, India

Keywords Iron ore geochemistry · Digital image processing · ASTER data · Geochemical anomaly · South India

Introduction

Satellite remote sensing techniques have played a predominant role in the geological prospecting of mineral deposits all over the globe (Divya et al., 2021; Gopinathan et al., 2020a, b; Kruse, 1995; Sabins, 1999; Yamaguchi et al., 2001). They can provide useful information about mineral exploration in short time as

well as in low price, and they are viable in regions with difficult accessibility to conduct field work (Yang et al., 2005; Sabins, 1999; Kruse & Prerry, 2006a; Gopinathan et al., 2020a, b). Multispectral ranges are useful in mapping of iron-bearing minerals, hydroxyl mineral, sulfates, and carbonates (Kiran Raj et al., 2015). Ramadan et al. (2009) combined the remote sensing tools such as the band ratio with lithological details in the successful prospecting of ferruginated beds in Owein at, El Dakhla district, western desert, Egypt. Revealing of the sites of ferruginated beds in the study area facilitated the field work and created further scope in the exploration and characterization of ferruginous minerals (Al-Quraishi et al., 2020). Magendran et al. (2011) successfully attempted to map and characterize different grades of iron ores in Noamundi and Joda area, eastern India. In their study, the authors have utilized certain key spectral parameters which were derived from laboratory-based spectral curves to correlate with the actual geochemical composition of the iron ores (Lanfranchi et al., 2020; Divya & Gopinathan, 2019; Divya et al., 2014a, b). In another study, Magendran and Sanjeevi (2013) demonstrated the importance of hyperspectral signatures obtained from the satellite imageries to evaluate the ranks of Fe-ore formations of Singhbhum iron ore belt in parts of Orissa and Jharkhand, eastern India, where they used Hyperion image data to detect iron ore deposits and its spatial extent (Farifteh et al., 2013; Mohamed et al., 2021). The multispectral or hyperspectral sensors and the laboratory-based discrete iron ore samples are effective to assess and characterize the iron ore deposits in an open mine-face (Magendran & Sanjeevi, 2014). Identification and delineation of the spatial distributions of iron deposits are crucial within the mineral exploration (Feizi & Mansouri, 2013). The satellite remote sensing product can support and help to do mapping of the mineral deposits in regional scale with adequate spatial and spectral elements (Oliver & vad der Wielen, 2005). The spectral signatures of multispectral data and hyperspectral data in 0.4–2.5 μm (VNIR-SWIR) provide direct detection of mineral. Such data, viz., ASTER, provide synoptic spatial coverage that allow extending the mineral targeting to regional scale and they lead to better mineral targeting over wider regions (Crosta et al., 2013; Kruse & Prerry, 2007b). Studies have also been conducted for mapping the lithological changes and mineral assemblages using the ASTER imagery in the granitic and meta-sedimentary

terrains as well as to measure the content of soil–water based on the hyperspectral remote sensing methods (Zhang et al., 2007; Haselwimmer et al., 2010; Salati et al., 2011; Ciampalini et al., 2012; Gad & Raef, 2012; Khidir & Babikir, 2013; Mishra et al., 2014; Dhivya & Gopinathan, 2019; Dhivya et al., 2021). This study aims to identify the iron-bearing mineral assemblages in soil and re-appraise the ferric, ferrous, and lateritic assemblages in iron-bearing soil of Nainarmalai, in north-western part of Tamilnadu, using ASTER image and chemical results of field specimens. This study uses state-of-the-art remote sensing strategies and different techniques such as band ratio, normalized difference vegetation index (ndvi), principal component analysis (PCA), and linear spectral unmixing (LSU). These techniques of satellite image data processing used in the exploration and identification of iron-bearing mineral assemblages in soil that conceal the iron reserve represented by the banded magnetite quartzites (Wan et al., 2021).

Geological system of study area

Nainarmalai is located at the northwest part of Tamil Nadu in southern India. This area is located at a distance of 11 km from Namakkal town and it forms part of the excessive grade granulite terrain (Fig. 1). It has structural hills consisting of linear ridges and few inselbergs. The linear ridges represent alternative bands of the banded magnetite quartzite (BMQ) (Gopinathan et al., 2015).

Nainarmalai is undoubtedly one of the low-grade iron ore formation in Tamil Nadu and. The BMQ occurs along with alternative bands of pyroxene granulite at northeast side of the “V”-shaped structural hill. The pyroxene granulite bands are associated with garnet-ferrous gneiss and quartzo-felspathic gneiss, pyroxenite, dolerite dyke, and pegmatite. The quartz veins occur as intrusive bodies. The area is structurally disturbed with repeated folding and NE-SW faulting and it is also subjected to granulite facies metamorphism as evidenced by the presence of amphibolite and pyroxene (Reddy et al., 1982). The banded iron ore formation varies in thickness from 2 to 20 mm. The total probable reserve of iron ore with 35 to 37% iron content is estimated to be around to be 8.2 million tons. It goes up to the depth of 30 m and contains two BMQ bands with strike length of 4.2 km

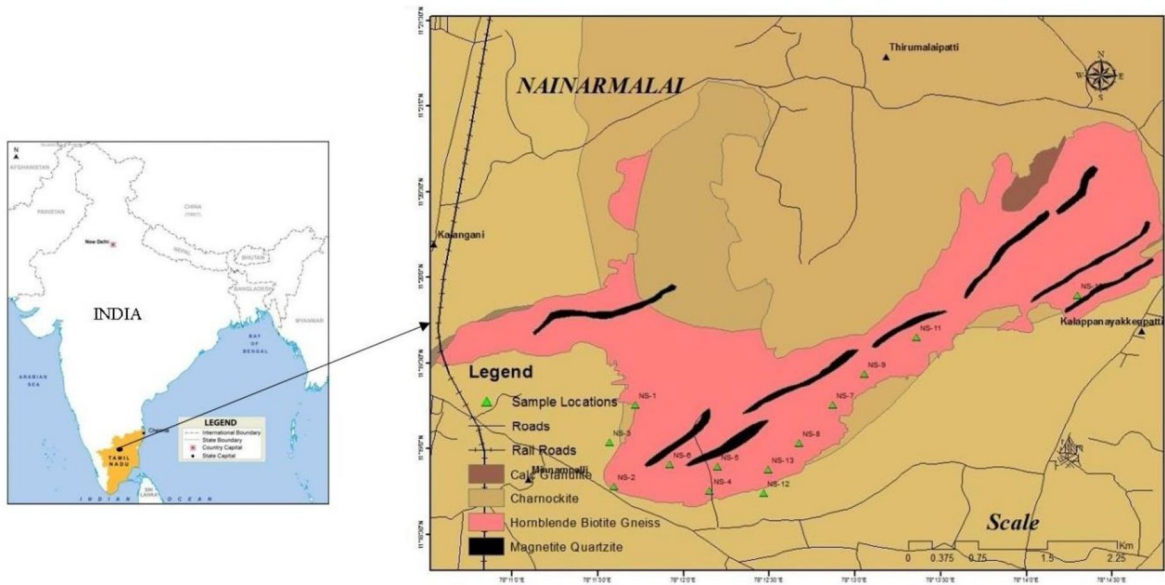


Fig. 1 Map showing the location of study area in southern India and different geological units

and average thickness of 25 m (GSI-2006). The top soils of iron-bearing mineral assemblages, however, conceal the entire study area. They vary over the space due to differential weathering process and we attempt to identification and delineation the iron-bearing top soils in this study.

Material and methodology

Our research methodology involved two essential components. The first one is Advanced Spaceborne Thermal and Emission Reflectance Radiometer (ASTER) satellite image processing such as preprocessing, band selection, 2-D scatter plot, ratio techniques, NDVI, and linear spectral unmixing techniques and interpretation of the results. The second one is field sample analysis that includes sample collection, sample preparation, and geochemical analysis of samples to decipher major iron-bearing mineral assemblages. Results of the above two components were compared and validated for mapping iron-bearing mineral assemblages in the top-soil. The overall methods used in this work are presented in Fig. 2.

In the digital processing techniques, we disposed or removed the errors pertaining to the data acquisition such as the atmospheric effects, to be able to improve the accuracy of mapping. The data provider, LP DAAC, United States Geological Survey (USGS) accomplished atmospheric correction and the processing strategies used in this research work.

Band selection and 2-D scatter plot

The space image plotted the data file value of one band against the values of another band (e.g., Kruse & Perry, 2006a). This 2D scatter plot displayed two bands of image pixel value in a Cartesian plot and illustrated the correlation between them. We selected ROI in the scatter plots and used them in other full band processing techniques. This study utilized the spectral property of iron oxide mineral in the scatter plots. The pixels containing iron oxide showed relatively strong absorption in the VNIR region and relative reflectance in the red band (Townsend, 1987; Shaik et al., 2021). The different bands of ASTER image were selected based on the scatted plots and the region representing iron oxide were identified. The newly created spectral subset consisted of the bands resembling iron oxide mineral assemblages and

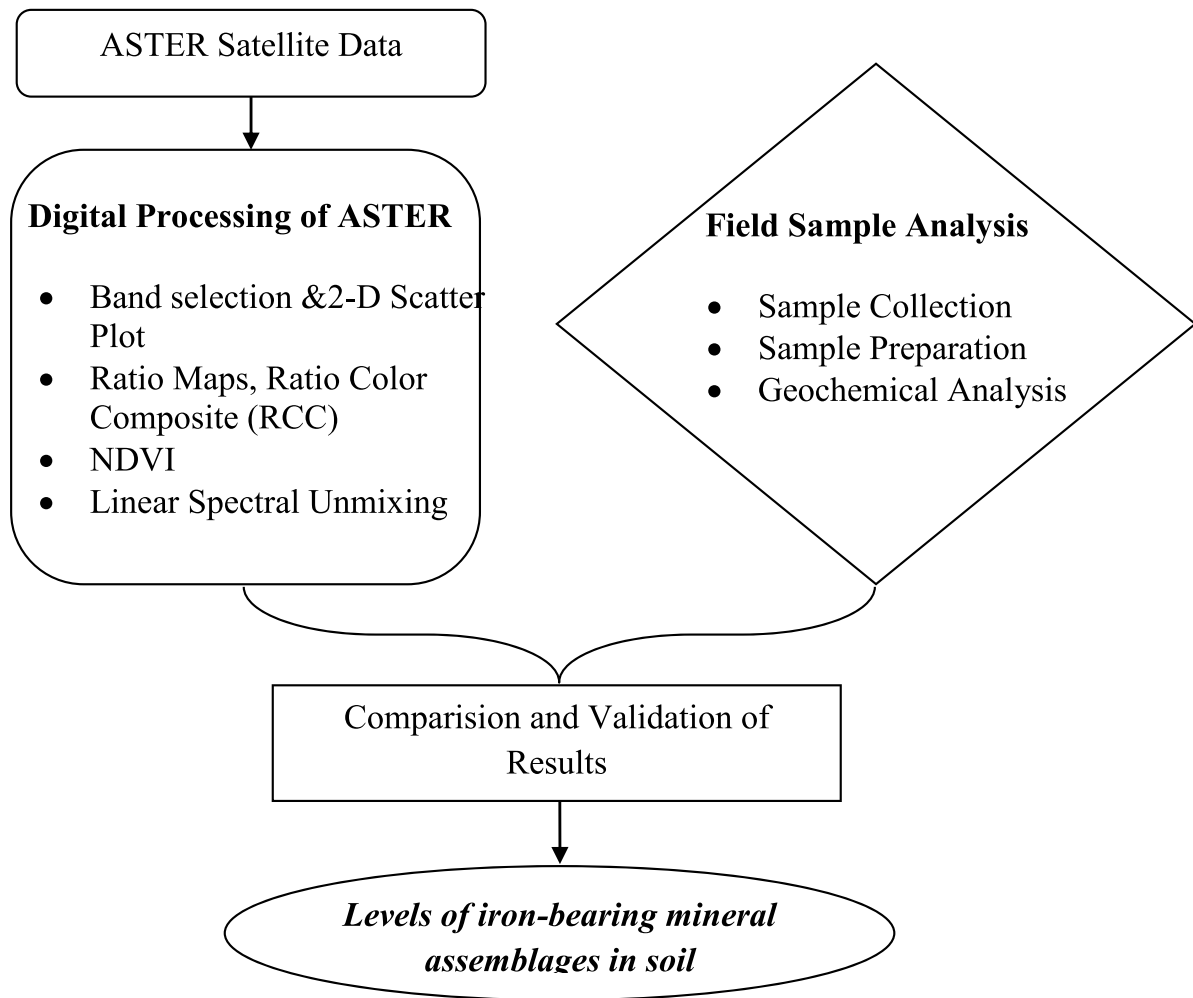


Fig. 2 Methodology flow chart of study

the spectral plot illustrated images illustrated different amounts of relative absorption and reflectance. The appropriate ASTER bands in the ratio analysis identified the signatures of iron oxides, vegetation, and country rocks (Madani & Emam, 2011).

Ratio analysis

Band ratioing is one of the simplest and dominant methods in satellite image processing. It emphasizes or exaggerates the mineral assemblages exist in the targeted regions (Khalaj et al., 2021). In this study, Fe-iron oxide minerals assemblages are the strategic target and we considered ratio images to improve spectral illustrations among the bands in the rationing and

mineral mapping (e.g., Elsayed & Albielyb, 2008). Every material has unique spectral characteristic (i.e., spectral reflectance) in different wavelength portions of electromagnetic spectral range. For example, the iron oxide shows absorption in 0.85–0.90- μm region of the electromagnetic radiation. Different band combinations are used in this study to delineate iron-bearing mineral assemblages. They are used to improve the spectral feature of alteration zones depending on the absorption bands of altered minerals (Gupta, 2003). We identified the following band ratio combinations to identify the iron oxide in soil: (i) (band 5/band 3)+(band 1/band 2) blend to delineate ferrous iron oxide, (ii) (band 2/band 1) combination to delineate ferric iron oxide, and (iii) (band 4/band 5) to delineate lateritic content.

Ratio color composite

Three primary colors (blue, green, and red) are considered for displaying color composite image. The merging of each spectral band combinations to a separate primary color mediums resulted in a color composite image to visualize iron-bearing mineral assemblages in a holistic view. Ratio process has made by dividing the brightness value of different bands and pixel by pixel. The primary concepts of ratios is to improve material contrast by dividing brightness values at peaks and troughs in a spectral reflectance curve. This has the effect of amplifying spectral differences while suppressing illumination differences (Herrera, 2015).

Normalized difference vegetation index

The relatively coarse resolution (15 m) ASTER image included the vegetation in the 1–10 m iron ore bands (e.g., Dalbin, 2008). The normalized difference vegetation index (NDVI) values ranging from 50 to 255 were categorized as dense vegetation in-and-around the study area. We grouped them in one class and created a mask for this NDVI category. Similar regions were masked from the original subset of ASTER image by using the image masking technique.

Linear spectral unmixing for estimation of iron-bearing mineral assemblages

The linear spectral unmixing method was used in iron mineral abundance maps, which combined with image spectra, aided in determining the grades of iron ores minerals in the study area. This analysis indicates the methodology's potential applicability for iron mineral identification and classifying grades of iron ores minerals (Kayet et al., 2017). It determined the comparative abundances of resources with different spectral characteristics in the multispectral/hyperspectral images. The reflectance at each pixel was considered as a linear permutation of reflectance of each substance end member, and it represented pure materials characteristics inside the pixel. There are, however, unique boundaries that follow for the linear spectral unmixing method. The amount of end members ought to be not up to the quantity of spectral bands and all the end members within the satellite imagery should be considered for the effective

plotting outcome. The outcome is extremely dependent on the contribution end members. Therefore, it is important to select end member spectra of pure materials such as iron-bearing mineral assemblages in soil and other country rock materials.

End-member selection by principal components analysis

Precise channels of multi-spectral images are incredibly compared and as a consequence include equivalent know-how. Image transformation procedures will also be utilized to lower this information dismissal and relationship between bands. (Geological Survey of Canada, 2004) has stated that principal components analysis (PCA) is one of the important transform methods. PCA, and different intricate transforms, could be utilized as an improvement manner to reinforce manual analysis. Otherwise, it could be utilized to scale back the total number of channels for use as enter to expertise extraction. In the end member assortment procedure that numerous end members has been preferred to determine the sub-categories of aim Fe-oxide minerals in soil and other formations each on the basis of exceptional combo of pixel parameters equivalent to size and density of the pixels and percent quilt, which lead to the variation of absorption and the value of reflectance in the spectra.

We validated and compared the abundances of iron-bearing mineral assemblages (i.e., high, medium and low levels) of the remotely sensed data (ASTER) with the actual geochemistry of field samples. Ground truth verification and sample collection formed important components of this research.

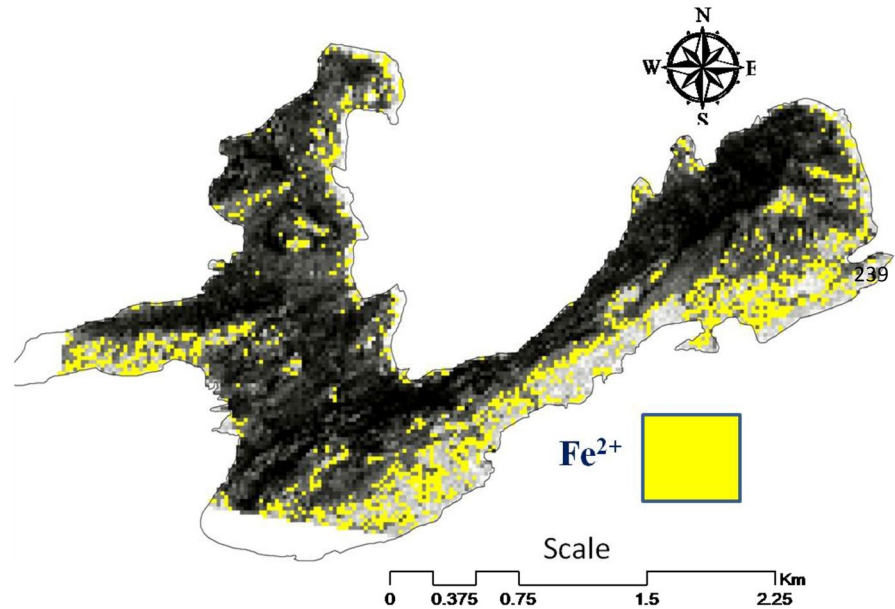
Result and discussion

The results obtained based on the above methodology including the satellite image processing techniques and geochemical analysis of the field samples are presented in this section and discussed successively.

Ferrous and ferric mineral assemblages

The bands 5/3 + band 1/2 ratio combination was computed to produce a map of ferrous mineral wealth (Fig. 3). Ratio images intended to demonstrate the spectral disparity of precise absorption

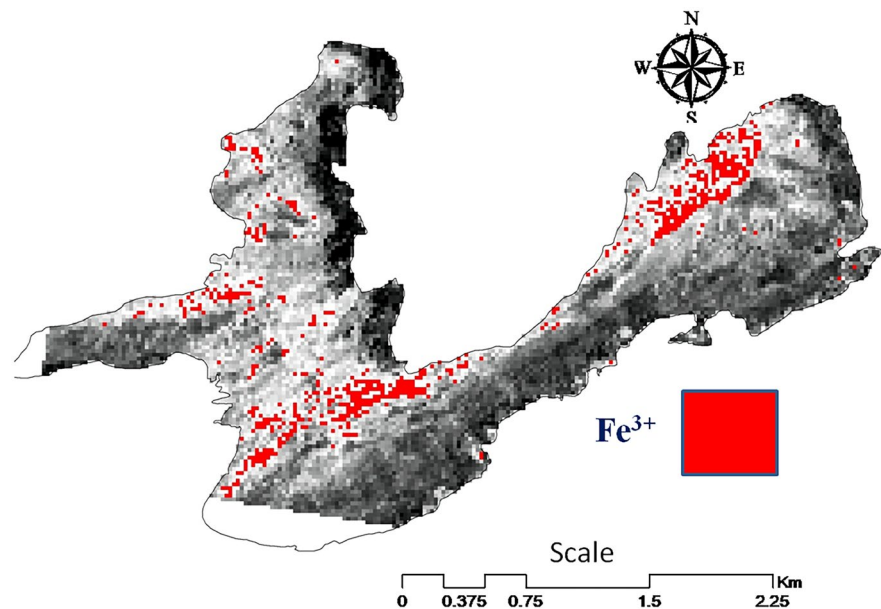
Fig. 3 Image showing ferrous mineral abundance



features that identified ferrous iron oxides highlighted in yellow color in the image output.

Similarly, the ferric mineral abundance map was generated using the band ratio combination of band 2/band 1. The resultant image exhibited variations in gray scales variations and high concentration of ferric iron contents in brighter pixels (red color in Fig. 4).

Fig. 4 Image showing ferric mineral abundance



Lateritic mineral assemblages in soil

The lateritic contents possess both the aluminum oxide and iron oxide. The sensitive bands indicating the aluminum oxide and iron oxide were identified through the 2D scatter plot. We generated the lateritic mineral distribution map using the ASTER bands ratio of band 4/band 5. Figure 5 shows the lateritic

Fig. 5 Image showing lateritic mineral abundance

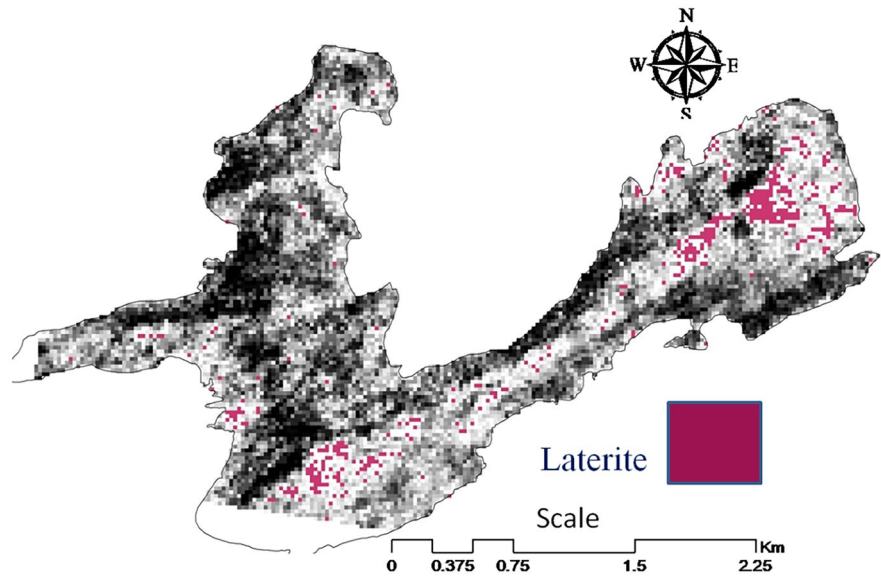


Fig. 6 Image showing ratio color composite of Nainarmalai

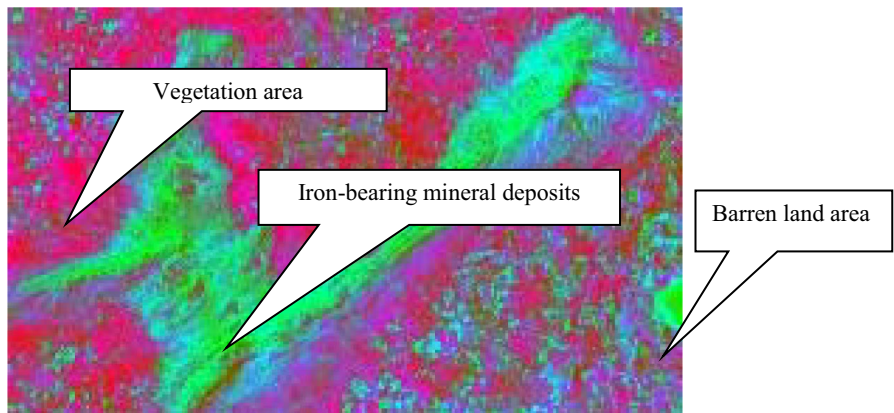


Fig. 7 Image showing NDVI of Nainarmalai

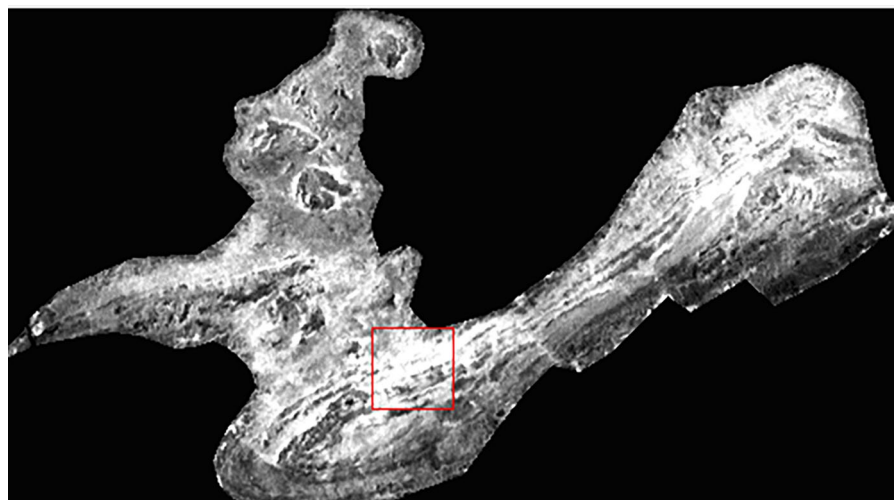


Fig. 8 Image showing vegetation masked ASTER image of Nainarmalai

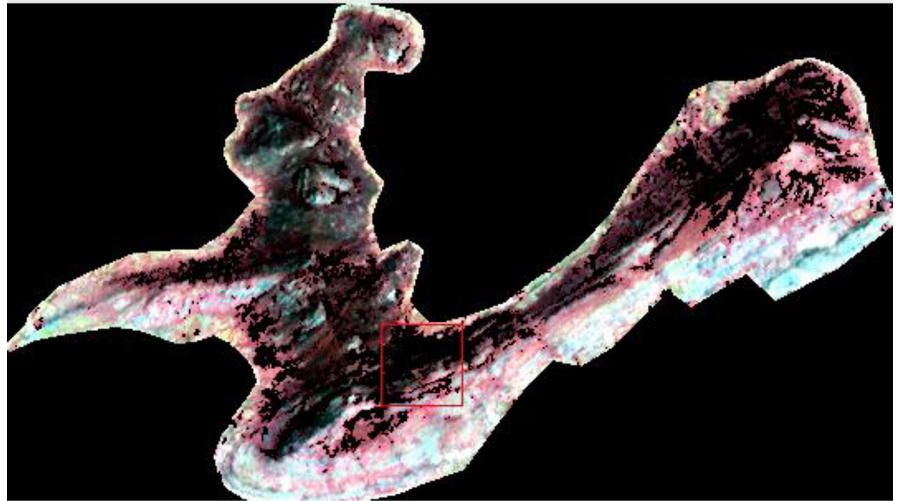


Fig. 9 End-member spectra of Nainarmalai

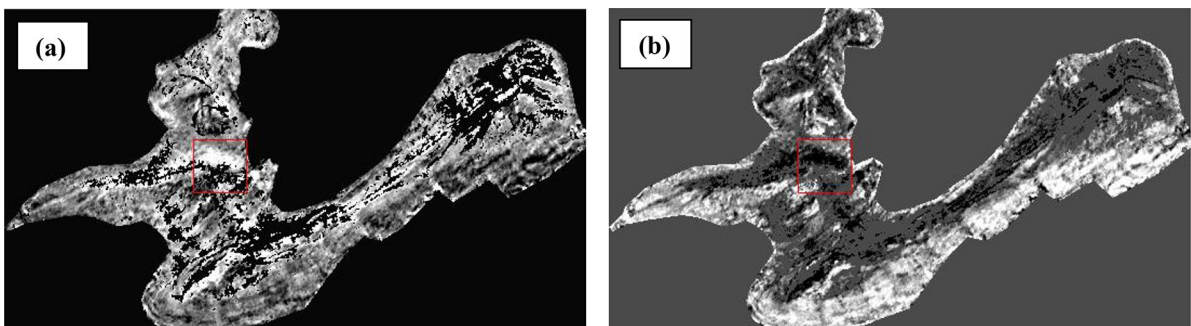
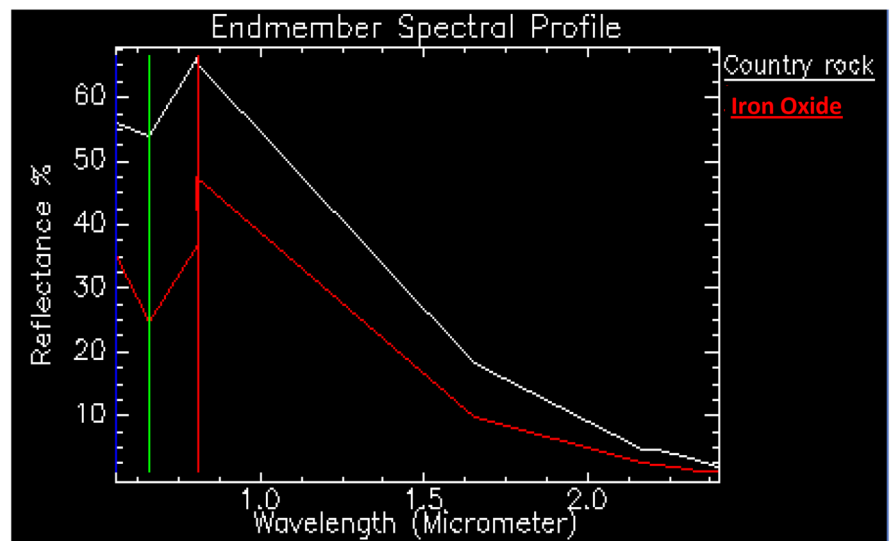


Fig. 10 **a** Iron oxide fraction image and **b** parent/country rock fraction image

Fig. 11 Image showing the categories of iron oxide content in soil of Nainarmalai area

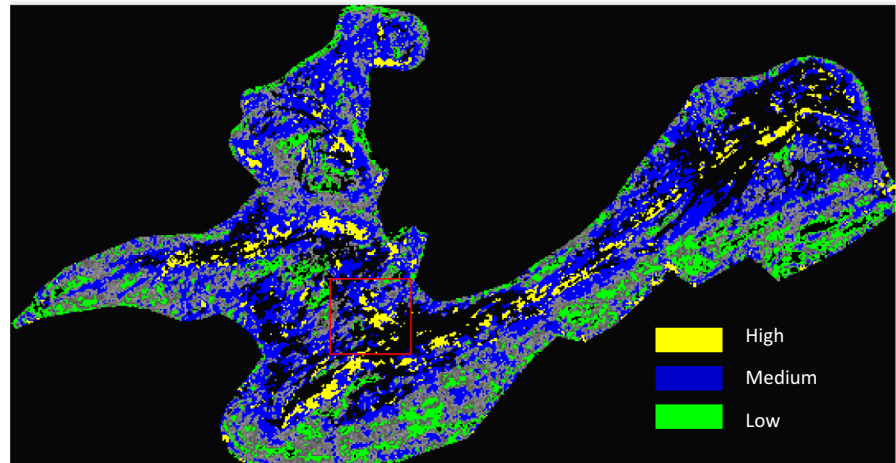


Fig. 12 Field photograph showing iron mineral assemblage in top-soil at Nainarmalai in southern India

mineral abundance of the study area highlighted in claret color.

Further, the color composite images were produced for delineating ferric, ferrous, and lateritic contents using the band ratio output images, such as band 5/3 + band 1/2, band 2/band 1, and band 4/band 5. The results were also verified with field check and chemical results of the specimens obtained in the field. The ratio color composite (RCC) maps presented better medium of visualization and interpretation to figure out the location and aerial extension of iron-bearing mineral assemblages, vegetation and barren land. The iron-bearing mineral assemblages in ridges were depicted in the RCC image (Fig. 6).

In accordance, there was interference by vegetation during mapping the iron-bearing minerals. We generated NDVI images to overcome interference of vegetation in the mapping (Fig. 7).

Subsequently, the vegetation content was identified and it was masked from the original image that contains either the iron-bearing mineral assemblages or country rocks (Fig. 8).

Then the resulted sub-categories had been mixed to receive the absolute end-member spectra of pure Fe-oxide and parent strata (determine 9). The golf green spectra signify Fe-oxide and white spectra characterize parent formations in the field of investigation (Fig. 9).

Fraction images

Fraction images have been created utilizing 2 end-member spectra, representing the iron oxides and other rocks. The pixel values indicated the richness of end member in the output fraction images. The pixel values varied from brighter to darker tones for the entire scene. These pixel fractions offered information about the relative abundance of end-member in a pixel. We used 2 individual end-members to obtain details to describe the resultant image (Fig. 10).

The fraction images of study area depicted the iron-bearing mineral assemblages and country rocks present in each pixel. Brighter pixels in the fraction images represented higher abundances. The peaks and ridges in the Fe-oxide fraction imageries showed most of the brighter areas and the hill slopes had the moderate abundance of iron oxide. The brighter areas in the other strata fraction imageries indicated parent rocks corresponding to garnet-amphibole and feldspathic gneisses, pyroxene granulites, amphibolites, and quartzites, and so forth.

Categorization of iron oxide distribution

Density chopping is one of the widely followed satellite image processing methods used to a single band monochrome image for highlighting the places having even tone. The grey-scale values (most commonly zero to 255 for 8-bit knowledge) are transformed to series distinctive slices and exceptional colors are allotted to every slice. To spotlight editions in the plant species,

this technique is mostly applied. We used this technique to highlight iron oxide variations in soil. The categorization image was generated using the iron oxide fraction image that provided relative abundance of iron oxide in each pixel. This in-turn showed the variation of iron oxide abundance in soil and we used this approach to demarcate the categories of high, medium and low levels of iron oxide contents (Fig. 11).

Geological sample collection and geochemical analysis

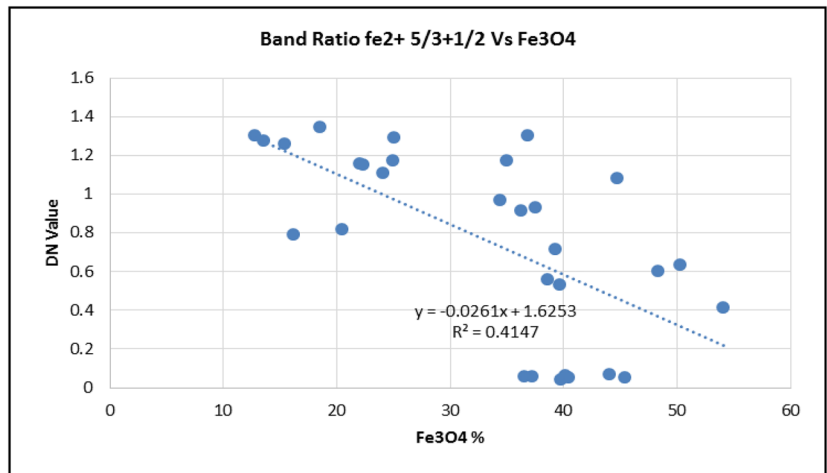
Based on the results of ASTER image processing and analysis of the study site, we took an extensive field survey for ground truth verification at random locations of the study area. The field verification was once carried out arbitrarily, and exceptional sampling locations have been identified utilizing a handled global positioning system (GPS). We collected 13 specimens from different places in the field of interest (Fig. 12) in order to come within the areas where the ASTER data processing and analysis identified the presence of iron oxide-bearing soil.

These samples were powered to 100-micron size for the geochemical analysis. All the powdered samples were analyzed with XRF to estimate the concentrations of the oxides of eleven different elements by following the standard procedures of (US EPA Method 6200, 2006; Kodom et al., 2012). Contents of Fe_3O_4 varied between 18.54 and 54.07% and Table 1 presents the concentrations of all the other oxides.

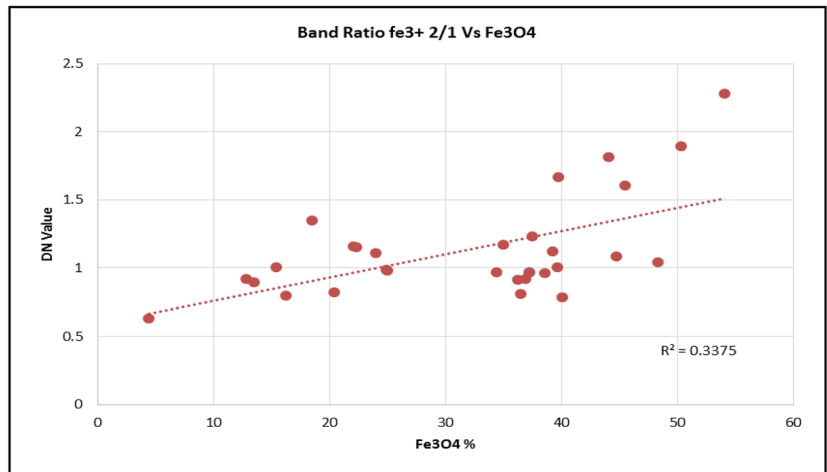
Table 1 Concentrations of different oxides including Fe_3O_4 in different field samples collect from the top-soil at Nainarmalai in southern India

S. no.	Sample ID	Sample locations		Concentration (%)										
		Latitude	Longitude	Al_2O_3	CaO	Fe_3O_4	K_2O	MgO	MnO	Na_2O	P_2O_5	SiO_2	SO_3	TiO_2
1	NS1	11° 19' 02.7"N	78° 12' 40.1"E	4.02	12	24.05	10.2	5.24	0.34	0.64	0.21	37.2	0.26	1.33
2	NS2	11° 18' 46.6"N	78° 11' 35.6"E	3.96	12.6	25.23	14.6	7.02	0.51	0.69	0.09	38.7	0.13	0.89
3	NS3	11° 18' 53.4"N	78° 12' 13.6"E	8.08	13.1	22.09	15.2	6.84	0.42	0.65	0.02	35.2	0.12	0.91
4	NS4	11° 18' 45.0"N	78° 12' 09.2"E	4.11	11	26.76	12.3	4.1	0.53	0.33	0.09	39	0.03	0.09
5	NS5	11° 18' 54.8"N	78° 11' 54.4"E	7.02	16.1	18.54	9.23	0.31	0.57	0.38	0.04	37.6	0.52	0.68
6	NS6	11° 18' 54.1"N	78° 11' 55.2"E	5.43	13.2	23.45	1.24	2.1	0.765	0.678	0.088	37.3	0.88	0.15
7	NS7	11° 19' 39.8"N	78° 13' 22.1"E	4.31	12.2	22.31	0.17	8.82	0.21	0.77	0.1	36.4	0.2	1.24
8	NS8	11° 19' 01.6"N	78° 12' 40.6"E	2.27	9.1	28.93	0.87	5.13	0.01	0.87	0.34	40.1	0.59	0.42
9	NS9	11° 19' 26.1"N	78° 13' 03.3"E	7.18	1.32	34.56	0.1	1.35	0.009	0.345	0.621	40	0.49	0.98
10	NS10	11° 19' 26.5"N	78° 13' 03.4"E	0.16	0.25	54.07	0	1.48	0.01	0	0.131	43.9	0	0
11	NS11	11° 19' 53.2"N	78° 14' 17.6"E	3.02	2.41	35.02	5.25	0.24	0.67	0.46	0.03	36.2	0.32	0.48
12	NS12	11° 19' 14.7"N	78° 12' 52.1"E	0.11	0.71	44.77	0.01	1.52	0.01	0.086	0.26	52.5	0	0
13	NS13	11° 18' 52.5"N	78° 12' 29.6"E	1.13	0.42	39.25	0.11	0.262	0.02	0.442	0.11	50.2	0.22	0.08

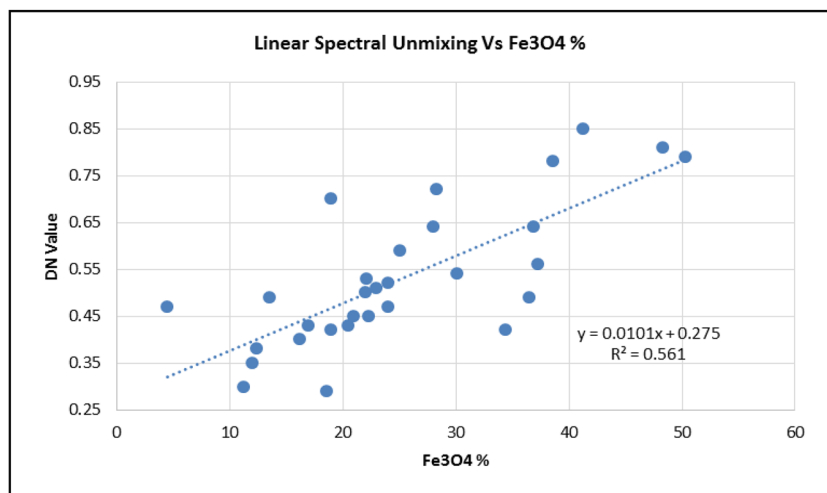
Fig. 13 Correlation of ASTER derived iron oxide abundance and the results of Fe3O4 estimated by geochemical analysis of field samples: **a** band ratio for ferrous oxide (Fe2+) vs Fe3O4 (%), **b** band ratio for ferric oxide (Fe3+) vs Fe3O4 (%), and **c** linear spectral unmixing for iron oxide vs Fe3O4 (%)



(a)



(b)



(c)

Correlation study

Band ratioing and linear spectral unmixing were used to categorize the iron oxide levels in soil samples (Fig. 13). The correlation of ASTER derived iron oxide abundance and actual Fe_3O_4 contents in field samples shows that the spectral unmixing techniques are capable of estimating the iron oxide levels with good correlation with an upright accuracy ($R^2=0.6$). The band ratio techniques have moderate positive and negative correlations with the iron oxide contents ($R^2=0.3$ and -0.4). Both the band ratio techniques were viable to identify and delineate ferrous, ferric and lateritic contents in the soil. The linear spectral unmixing techniques, however, were reliable in the context of mapping the distribution of iron-bearing mineral assemblages in soils of the study area.

Conclusions

The spectral analysis and software-based image interpretation of ASTER data has given important evidence to estimate the abundance of Fe-bearing minerals in top soil of the granulite terrain at Nainnarmalai in southern India. This area has probable reserve of commercially exploitable iron ore in the forms of banded magnetite quartzites. Band rationing techniques with specific band combinations, such as band 2/band 1 (for ferric), band 5/band 3 + band 1/band 2 (for ferrous), and band 4/band 5 (for laterite), estimated the abundances of iron oxide in the top-soil. The fraction images resulted from linear spectral unmixing delineated the Fe-oxide and parent rocks. Fe-oxide fraction image indicated higher abundance at ridges and moderate abundance at slopes. Likewise, the brighter pixels in parent strata fraction images characterized garnet-amphibole and feldspathic gneisses, pyroxene granulites, amphibolites, and quartzites. The comparison of the outcomes of chemical results of specimens randomly obtained in the field and the corresponding iron oxide wealth resulted from linear spectral unmixing inferred that the spectral unmixing techniques of the ASTER data are capable of estimating iron oxide levels in the soil with good correlation ($R^2=0.6$). Based on the results of this study, we concluded that it is possible to detect iron oxide content in the soil samples and assess the spatial distributions of ferrous, ferric, and lateritic areas from the

ASTER image data. The linear spectral unmixing tools in satellite image processing were helpful to categorize the Fe-oxide abundances with reasonable accuracy and minimal requirement of ground truth.

Acknowledgements Authors are grateful to the Director, CSIR-Central Institute of Mining & Fuel Research (CSIR-CIMFR), Dhanbad, for constant support. The authors are thankful to the Commonwealth Scientific and Industrial research organization for the open source information used in this study.

Declarations

Conflict of interest The authors declare no competing interests.

References

- Al-Quraishi, A., Mustafa, B., Gopinathan, P., & Yuvaraj, D. (2020). potential of multispectral satellite data for superficial iron oxide detection in Sulaimaniyah, Iraqi Kurdistan Region. *Journal of Geoinformatics & Environmental Research*, 1(1), 46 - 57. <https://doi.org/10.38094/jgier1117>
- Ciampalini, A., Francesca, G., Benedetta, A., Sandro, M., & Gaia, R. (2012). Remote sensing techniques using Landsat ETM+ applied to the detection of iron ore deposits in Western Africa. *Arabian Journal of Geoscience*, 12517–012–0725–0.
- Crosta, A. P., & De Souza Filho, C. R. (2013). Targeting key alteration minerals in epithermal deposits in Patagonia, Argentina, using ASTER imagery and principal component analysis. *International Journal Remote Sensing*, 24(21), 4233–4240.
- Dalbin. (2008). Processing of multispectral and hyperspectral images for iron ore studies a thesis submitted to the faculty of science and humanities in partial fulfillment of the requirement for the degree of Master of Science in applied geology.
- Divya, Y., & Gopinathan, P. (2019). Soil water content measurement using hyper-spectral remote sensing techniques – A case study from North-Western Part of Tamil Nadu, India. *Society and Environment*. <https://doi.org/10.1016/j.rsase.2019.01.005>
- Divya, Y., Gopinathan, P., Jayachandran, K., et al. (2021). Color slices analysis of land use changes due to urbanization in a city environment of Miami Area, South Florida, USA. *Modeling Earth Systems and Environment*, 7, 537–546. <https://doi.org/10.1007/s40808-020-00883-x>
- Divya, Y., Sanjeevi, S. & Ilamparuthi, K. A. (2014a). study on the hyperspectral signatures of sandy soils with varying texture and water content. *Arabian Journal of Geoscience*, 7, 3537–3545. <https://doi.org/10.1007/s12517-013-1015-1>
- Divya, Y., Sanjeevi, S. & Ilamparuthi, K. (2014b) Studies on textural and compositional characteristics of sand and clay mixtures using hyperspectral radiometry. *Journal of Indian Society Remote Sensors*, 42, 589–600. <https://doi.org/10.1007/s12524-013-0336-6>

- Elsayed Zeinelabdeina, K. A., & Albielyb, A. I. (2008). Ratio image processing techniques: A processing tool for mineral deposits, red sea hills, NE Sudan. *International Archives of the Photogrammetry, Remote Sensing and Spatial Information Science*, XXXVII(B8), Beijing.
- Farifteh, J., Nieuwenhuis, W., & García-Meléndez, E. (2013). Mapping spatial variations of iron oxide by-product minerals from EO-1 Hyperion. *International Journal of Remote Sensing*, 34(2), 682–699. <https://doi.org/10.1080/01431161.2012.715776>
- Feizi, F., & Mansouri, E. (2013). Introducing the iron potential zones using remote sensing studies in South of Qom Province, Iran. *Open Journal of Geology*, 3(4), 278–286. <https://doi.org/10.4236/ojg.2013.34032>
- Gad, S., & Raef, A. (2012). Factor analysis approach for composited ASTER band ratios and wavelet transform pixel-level image fusion: lithological mapping of the Neoproterozoic Wadi Kid area, Sinai, Egypt. *International Journal of Remote Sensing* 33(5), 1488–1506. <https://doi.org/10.1080/01431161.2011.577106>
- Geological Survey of Canada. (2004). Remote sensing and geosciences.
- Geological survey of India. (2006). Detailed information dossier (did) on iron ore in India.
- Gopinathan, P., Mohan, S. P., & Magendran, T. (2015). Structural, mineralogical and ore grades of banded iron deposits of north-western Tamil Nadu, South India – A comparative study. *International Journal of Emerging Technology and Advanced Engineering*, 5(3).
- Gopinathan, P., Parthiban, S., Magendran, T., Al-Quraishi, A. M. F., Singh, A. K., & Singh, P. K. (2020a). Mapping of ferric (Fe³⁺) and ferrous (Fe²⁺) iron oxides distribution using band ratio techniques with ASTER data and geochemistry of Kanjamalai and Godumalai, Tamil Nadu, south India. *Remote Sensing Applications: Society and Environment*, 18, 100306. <https://doi.org/10.1016/j.rsase.2020a.100306>
- Gopinathan, P., Nandini, C. V., Parthiban, S., Sathish, S., Singh, A. K., & Singh, P. K. (2020b). A geo-spatial approach to perceive the groundwater regime of hard rock terrain- A case study from Morappur area, Dharmapuri district. *South Indian Groundwater Sustained Development*, 10.
- Gupta, R. P. (2003). *Remote sensing Geology* (2nd ed.). Springer.
- Haselwimmer, C. E., Riley, T. R., & Liu, J. G. (2010). Assessing the potential of multispectral remote sensing for lithological mapping on the Antarctic Peninsula: Case study from eastern Adelaide Island, Graham Land. *Antarctic Science*, 22(3), 299–318.
- Herrera, G. J. J. (2015). Mapping iron bearing orrormation using hyperspectral and multispectral images. A Case Study of Singhbhum - Keonjhar Iron Belt - India.- *Geologia Colombiana*, 40. Bogotá, Colombia D.C.. pp.61–78.
- Kayet, N., Pathak, K., Chakrabarty, A., & Sahoo, S. (2017). Hyperspectral image analysis for iron mineral exploration and spectral unmixing study in Kiriburu and Meghahataburu Mining Areas, West Singbhum, Jharkhand. In *38th Asian Conf. Remote Sens.-Space Appl.: Touching Human Lives, ACRS*.
- Khalaj, M., Karimi, Z., & Rabbani, M. (2021). The exploration of metallic deposits using satellite image processing in the Parwan-Panjsher Area. *Afghanistan. Environ. Sci. Proc.*, 6, 30. <https://doi.org/10.3390/iecms2021-09354>
- Khidir, S., & Babikir, I. A. (2013). Digital image processing and geospatial analysis of landsat 7 ETM+ for mineral exploration, Abidiya area, North Sudan. *International Journal of Geomatics and Geosciences*, 3, 645–658.
- Kiran Raj, S., Ahmed, S. A., Srivatsav, S. K., & Gupta, P. K. (2015). Iron oxides mapping from EO-1 hyperion data. *Journal of the Geological Society of India*, 86(6), 717-725.
- Kodom, K., Preko, K., & Boamah, D. (2012). X-ray fluorescence (XRF) analysis of soil heavy metal pollution from an industrial area in Kumasi, Ghana. *Soil and Sediment Contamination: An International Journal*, 21(8), 1006–1021. <https://doi.org/10.1080/15320383.2012.712073>
- Kruse, F. A., & Perry, S. L. (2006a). Regional mineral mapping by extending hyperspectral signatures using multi-spectral data. IEEEAC paper #1078, Version 4, Updated November 24, 2006a.
- Kruse, F. A., & Perry, S. L. (2007b). Regional mineral mapping by extending hyperspectral signatures using multi-spectral data. IEEEAC paper #1078, Version 4, Updated November 24, 2006b.
- Kruse, F. A., (1995). Advances in hyperspectral remote sensing for geologic mapping and exploration. *Analytical Imaging and Geophysics LLC*.
- Lanfranchi, R. A., Cruz, S. C. P., & Rocha, W. F. (2021). Application of remote sensing and reflectance spectroscopy to explore iron-enriched domains in the north region of the intracontinental sector of the Araçuaí West Congo Orogen. *Ore Geology Reviews*, 128, 103916. <https://doi.org/10.1016/j.oregeorev.2020.103916>
- Madani, A. A., & Emam, A. A. (2011). SWIR ASTER band ratios for lithological mapping and mineral exploration: A case study from El Hudi area, southeastern desert, Egypt. *Arabian Journal of Geoscience*, 4, 45–52.
- Magendran, T., Sanjeevi, S., & Bhattacharye, A. K. (2011). Hyperspectral radiometry to quantify the grade of iron ore of Noamundi and Joda Mines, Eastern India. *Journal of Indian Soc Remote Sensing*, 39(4), 473–483.
- Magendran, T., & Sanjeevi, S. (2013). A study on the potential of satellite image-derived hyperspectral signatures to assess the grades of iron ore Deposits. *Journal of Geological Society of India*, 82, 227–235.
- Magendran, T., & Sanjeevi, S. (2014). Hyperion image analysis and linear spectral unmixing to evaluate the grade of iron ores in parts of Noamundi, eastern India. *International Journal of Applied Earth Observation and Geoinformation*, 26, 413–426.
- Mishra, B. K., Pattanayak, S., & Rautray, S. (2014). Geospatial and geological mapping of iron ore prospective zones in singbhum keonjhar belt Orissa. *Standard Global Journal of Scientific Research*, 1(1), 0123–019, Feb 2014.
- Mohamed, M. T. A., Al-Naimi, L. S., Mgbejedo, T. I., & Agoha, C. C. (2021). Geological mapping and mineral prospectivity using remote sensing and GIS in parts of Hamissana, Northeast Sudan. *J Petrol Explor Prod Technol*, 11, 1123–1138. <https://doi.org/10.1007/s13202-021-01115-3>
- Oliver, S., & van der Wielen, S. (2005). Mineral mapping with ASTER. *AUSGEO News*, (82), June 2005.
- Ramadan, T. M., Kelani, E. L., & A.H., Hassaan, M.M. and Salem, M.S., (2009). Use of remote sensing and geological

- studies in the exploration for iron deposits in the Oweinat, El Dakhla District, Western Desert, Egypt. *Australian Journal of Basic and Applied Sciences*, 3(1), 254–266.
- Shaik, I., Begum, S. K., Nagamani, P. V., Kayet, N. (2021). Characterization and mapping of hematite ore mineral classes using hyperspectral remote sensing technique: a case study from Bailadila iron ore mining region. *SN Applied Sciences*, 3, 182. <https://doi.org/10.1007/s42452-021-04213-3>
- Reddy, N. S., Reddy, V. P., Annamalai, A., & Prasad, C. V. R. K. (1982). Mineralogy and chemistry of the iron ores of Nainamalai, Tamilnadu. *Proceedings of the Indian Academy of Sciences-Earth and Planetary Sciences*, 91(1), 55–63.
- Sabins, F. F. (1999). Remote sensing for mineral exploration. *Ore Geology Reviews*, 14, 157–183.
- Salati, S., Frank, J. A., van Ruitenbeek, F. D., van der Meera, M., Tangestani, H., & van der Werff, H. (2011). Lithological mapping and fuzzy set theory: Automated extraction of lithological boundary from ASTER imagery by template matching and spatial accuracy assessment. *International Journal of Applied Earth Observation and Geoinformation*, 13, 753–765.
- Townsend, T. E. (1987). Discrimination of iron alteration minerals in visible and near-infrared reflectance data. *Journal of Geophysical Research*, 92(B2), 1441–1454. <https://doi.org/10.1029/JB092iB02p01441>
- US EPA Method 6200. (2006). ITRV: XRF technologies for measuring soil and sediment (NitonXLt 700 Series XRF). EPA publication EPA/540/R-06/004.
- Yang, J., Zhang, Y., Wu, H., Deng, G., & Li, M. (2005). New exploration developments using a new exploration parameter (Alteration Remote Sensing Anomaly) for metallic deposits in East Tianshan. In their book Chapter 14–13.
- Yu-Qing, W., Yu-Hai, F., & Mou-Shun, Ji. (2021) Application of hyperspectral remote sensing for supplementary investigation of polymetallic deposits in Huanishan ore region, northwestern China. *Science Representative*, 11, 440. <https://doi.org/10.1038/s41598-020-79864-0>
- Zhang, X., Pazner, M., & Duke, N. (2007). Lithologic and mineral information extraction for gold exploration using ASTER data in the south Chocolate Mountains (California). *ISPRS Journal of Photogrammetry and Remote Sensing*, 62, 271–282.
- Yamaguchi, Y., Fujisada, H., Tsu, H., Sate, I., Watanabe, H., Kate, M., Kudoh, M., Kahlc, A. B., & andPniel, M. (2001). Aster early image evaluation. *Advance in Space Research*, 28(1), 69–76.

Publisher's Note Springer Nature remains neutral with regard to jurisdictional claims in published maps and institutional affiliations.

Springer Nature or its licensor holds exclusive rights to this article under a publishing agreement with the author(s) or other rightsholder(s); author self-archiving of the accepted manuscript version of this article is solely governed by the terms of such publishing agreement and applicable law.